

Step edges on galena (100): Probing the basis for defect driven surface reactivity at the atomic scale

UDO BECKER^{1,*} AND KEVIN M. ROSSO²

¹Institut für Mineralogie, Universität Münster, Corrensstr. 24, D-48149 Münster, Germany

²W.R. Wiley Environmental Molecular Sciences Laboratory, Pacific Northwest National Laboratory, P.O. Box 999, MSIN K8-96, Richland, Washington 99352, U.S.A.

ABSTRACT

Scanning tunneling microscopy (STM) images of the PbS (100) surface with a step and several kinks were obtained with atomic resolution. These images show an increased tunneling current at step edge sites and an apparent deformation of the lattice near the step. The experimental images are compared with theoretical *ab initio* calculations for which we developed a hybrid method of constant current and constant height mode STM image simulation. With these calculations, we find that the apparent deformation is mainly an electronic effect rather than relaxation of atoms. In addition, with the help of these calculations, we can identify the changes of individual terrace-like and step-like orbitals that are observed using the STM in terms of the energy, density and shape of these states. This detailed knowledge of the electronic behavior of the PbS surface near a step can be used as a basis for explaining adsorption, acid/base, and redox behavior on PbS terraces and at steps, and the differences between the two.

INTRODUCTION

Since the invention of scanning probe microscopy techniques, it has become increasingly obvious that the reactivity of mineral surfaces is often controlled by the reactivity of surface steps. This can be the case, e.g., for growth and dissolution processes (Dove and Hochella 1993; Stipp et al. 1994; Bosbach et al. 1995; Dove and Platt 1996; Jordan and Rammensee 1996, 1998). For most growth mechanisms, such as layer-by-layer growth and spiral growth, atoms and molecules from solution adsorb to the mineral surface at step edges that bound growth islands and spirals (Pina et al. 1998). Reactions at step edges become even more important when ions from background electrolytes (Bosbach et al. 1996; Risthaus et al. 2001) and growth inhibitors or organic molecules that may be involved in biomineralization processes selectively adsorb to specific crystallographically oriented steps and control crystal growth rates and morphologies (Bosbach and Hochella 1996; Teng and Dove 1997). Reactions at steps are particularly interesting if adsorption is coupled with redox processes (Eggleston et al. 1996; Becker et al. 2001). Junta and Hochella (1994) have shown that the initial Mn adsorption from solution on hematite (001) surfaces predominantly takes place on surface steps. Becker et al. (1996) have described the differences between the electronic structure of flat terraces and step edges on hematite (001) in detail. This helps to explain why electron transfer from the Mn oxyhydroxide complex to oxygen via the hematite surface is enhanced at the step and thus, why the Mn oxidation from Mn²⁺ in solution to Mn³⁺ in

the adsorbed state is increased with respect to the adsorption at a flat terrace.

With respect to the PbS (100) surface, there have been several studies that indicate an increased tendency to react at step edges relative to flat terraces. Theoretical calculations have shown that although water preferentially physisorbs to flat PbS terraces (a weakly bound but structurally intact state), sorption to steps leads to rapid dissociation of the water molecules (Wright et al. 1999a, 1999b; Bryce et al. 2000).

In terms of the reactivity of steps, it is interesting to note that Vaitkus et al. (1998, 1999) found that the growth of galena clusters on a semiconducting Si surface is dependent on the surface morphology, especially, if the clusters grow on surface steps of the substrate. Thus, for the interfacial growth of one solid on another, the step reactivity of both substrates can play an important role for the nucleation of growth.

An elegant experimental technique to observe dissolution at atomic resolution is the Electrochemical STM (ECSTM, Higgins and Hamers 1995, 1996a, 1996b). Dissolution experiments on galena, pyrite and covellite using the ECSTM suggest that the formation of a single vacancy or of an initial microscopic etch pit and, thus, the formation of surface steps may be rate limiting during dissolution under acidic conditions (Higgins and Hamers 1996a). For galena, it was observed that in acidic conditions, dissolution occurs by selective removal of step edge species. Higgins and Hamers (1995) discussed crystallographic effects in terms of atomic structures of the step edges, but in the current study, evidence is found that electronic structure changes associated with different steps may be even more important.

Experimental and theoretical investigations of the electronic structure of PbS surfaces were performed by Tossell and

* E-mail: ubecker@uni-muenster.de

Vaughan (1987), Eggleston and Hochella (1993, 1994), Laajalehto et al. (1993), Becker and Hochella (1996), Bottner et al. (1996), Mian et al. (1996), Eggleston (1997), and Becker et al. (1997a, 1997b). It was found that the top of the valence band is dominated by combined S $3p_z$ -Pb $6p$ states where the states with S $3p_z$ character extend into the vacuum or the solution that is in contact with the surface. The states that are close to the Fermi level are the ones that are most important for redox reactions, and are analogous to the frontier molecular orbitals in molecules. Thus, oxidation reactions on the PbS surface are likely to be initially controlled by the shapes and density of states (DOS) of the orbitals with S $3p_z$ character. Accordingly, STM images at negative sample bias voltages mainly "pick up" S $3p_z$ electron density from sulfur atoms. In contrast, STM images at positive sample bias voltages probe the bottom of the conduction band, which is dominated by Pb $6p$ -like states and which are mainly responsible for nucleophilic reactions at the PbS surface. In this study, we show that these surface electronic properties are significantly modified at surface steps, and use this information to explain why certain reactions take place preferentially at these surface sites.

The mechanism of adsorption to PbS surfaces is also important in sulfide flotation processes with different collector molecules such as mercaptobenzothiazole and its derivatives (Maier and Dobias 1997; for a review in recent advances in flotation chemistry, see Woods 2000) or xanthate and dithiophosphate derivatives (Persson 1994). Especially at low dosages that are applied for economic reasons, or because of the toxicity of the collector molecules, understanding the physical basis underlying step-adsorbate interaction may be particularly important because at low concentrations, a high percentage of the molecules may be attached to surface steps due to their increased reactivity. Such an understanding begins with an analysis of the structure and electronic properties at the step edge. Other structural defects or impurities at the surface can have a similar effect in terms of an increased surface reactivity.

Finally, because many sulfide surface reactions are enhanced by microbial interaction (Fowler and Crundwell 1999; Holmes et al. 1999; Sharma and Rao 1999; Wieland and Kuhl 2000; Sampson et al. 2000; Santhiya et al. 2000; Wang et al. 2000), the redox processes that occur at steps, including the redox changing properties of bacteria, may be an interesting field for future research.

EXPERIMENTAL METHODS

The ultra-high vacuum (UHV) instrumentation and experimental methods used in this study are described in detail elsewhere (Rosso et al. 1999a, 1999b). Briefly, natural single crystals of galena were cleaved in a UHV load-lock chamber at a pressure of less than 10^{-7} mbar. Cleaving was performed using an in-house cleavage stage designed to produce well controlled cleavage along (100) planes of galena. Cleaved samples were immediately transferred into an ambient temperature UHV STM (Omicron, Inc.) in the main chamber at a base pressure of 10^{-10} mbar. Low energy electron diffraction images of the sample indicated that the surface was well ordered. STM tips were produced by electrochemical etching tungsten wire in 1

M KOH using AC current. Topographic (feedback signal) and current (error signal) images were collected in the dark using 0.25 V sample bias and 1 nA setpoint current. Filtering was accomplished using a low pass Fast-Fourier-Transform (FFT)-filter.

COMPUTATIONAL METHODS

General procedure

We used a cluster and a periodic two-dimensional quantum mechanical approach to evaluate the electronic and atomic structure near steps and to calculate STM images for tip positions above the near-surface region. In general, the calculation of STM images using a cluster approach follows the methods described in Becker and Hochella (1996) and Becker et al. (1997a). Calculation of the wavefunctions in the substrate was performed using the program package Gaussian98 (Frisch et al. 1998) with the option to embed the cluster in point charges to minimize edge effects, as described in Becker et al. (1997a). In addition to the point charge embedding, the contributions of the wavefunctions of neighboring clusters that are not contained in the actual Gaussian98 calculations were taken into account (Becker et al. 1997a).

Constant current STM images

In contrast to our previous studies (Becker and Hochella 1996; Becker et al. 1997a), constant current images were calculated in addition to constant height images. For constant current images, an imaginary tip is placed at about 5000 different (x,y) positions, 10 \AA (z) (where x,y is defined as being parallel to the surface, z perpendicular to the surface) above the cluster with a grid spacing of $\sim 0.1 \text{ \AA}$. Then, this virtual tip approaches the surface in constant steps of $\Delta z = 0.2 \text{ \AA}$ until a previously given value of I_{theo} with

$$I_{\text{theo}} = \sum_{E > -eV_{\text{bias}}}^{E_F} |\Psi(E, x, y, z)|^2 \quad (1)$$

is obtained. In Equation 1, a z position of the tip has to be found such that the sum over the densities ($|\Psi|^2$) of all states with energy eigenvalues (E) between $e \times$ (bias voltage, V_{bias}) to the Fermi level (E_F) has to equal I_{theo} which is the value of a theoretical tunneling current that is applied to the whole image (similar to the setpoint current in an experimental image). Equation 1 is for negative bias voltages; for positive bias voltages, the summations runs from E_F to eV_{bias} . The theoretical setpoint current is in arbitrary units because the actual tunneling current also depends on the atomic and electronic structure of the tip, which is not known. Note that in Equation 1, one would also have to sum over the k -points, if a calculation is performed with periodic boundary conditions. Once a sample-tip separation (z) is reached where the sum over the density of states is $\approx I_{\text{theo}}$, a Newton-Raphson-like algorithm is used to find a tip position which exactly satisfies Equation 1. Using this approach, there is a problem when the electronic structure near a surface step is evaluated. On the side of the lower terrace of such a step (about 2 \AA away from the step), there are lateral (x,y) positions of the tip that can have local minima in the z direction (usually not more than one for a monoatomic step) of the den-

sity of states and, thus, there may be two z positions (one above and one below the step) for which Equation 1 is fulfilled. This phenomenon can be thought of as a small "vertical cleavage plane" at steps with local maxima and minima. Therefore, it is necessary in the first approach to move the tip closer to the surface than to the first z in order to find all tip positions with that condition. In these cases, the software picks the position that is closer to the surface.

In experimental STM images, one never obtains ideal constant height or constant current images. Especially near step sites, it is not desirable to turn off the feedback loop for constant height images because the tip may crash into the step. In order to achieve perfect constant current mode, the electronics and mechanics of the instrument would have to react infinitely fast to follow topographic changes of the sample. Because we have now developed the methodology to calculate both modes, we are also able to combine these. The way we achieve this goal is to begin by calculating the z positions of all (x,y) positions in constant current mode. The next step is to apply a scheme to average these z values over a certain region about a given lateral (x,y) position. As a rule of thumb, the lower the feedback in the experimental setup, the larger the area needed to average the z values. In our calculations of theoretical STM images of the cluster setup (see below), we chose to average the z positions of the tip over the whole length of the cluster parallel to the step and over 1 Å left and right of a given (x,y) position perpendicular to the step. In this way, we obtain a plane for tip movement that is almost flat and at a certain distance (≈ 2.5 Å away from the sample) above the upper and lower terrace. In the vicinity of the step, the path of the theoretical tip describes a curved surface about the step. Then, we let the (theoretical) tip scan along this plane and calculate the tunneling current as a function of the (x,y) positions of the tip.

Such an approach for (more realistic) constant current mode STM simulations has the advantage of more closely mimicking the experimental scanning modes and allows the user to evaluate the electronic structure of the upper and lower terrace and of the step in one single theoretical image. For ideal constant height mode simulations, only the electronic structure of the upper terrace can be represented in the theoretical image. This is because for tip positions above the lower surface, the tip-sample separation would be the tip-sample separation above the upper surface plus the step height (≈ 3 Å in the case of PbS). Because of the exponential dropoff of the tunneling current as a function of the tip-sample separation, ideal constant height mode simulations above the lower surface would appear to be dark.

It has to be noted that this technique makes no assumption about real tip morphology. That means, for instance, that the curvature of the virtual tip is infinitely small and no additional "rounding" of the step is applied due to a finite tip curvature.

Clusters and periodic models

The cluster calculations were performed with and without surface and step relaxation. This allows one to distinguish between effects on the STM image that are caused solely by electronic structure changes near steps and those that are caused by electronic and atomic structure changes.

Calculations with periodic boundary conditions were performed using the program package Crystal98 (Dovesi et al. 1999). Basis sets were structure and energy optimized from a Durand and Barthelat basis set that was developed in combination with the Durand pseudopotential set. We used these pseudopotentials to mimic how the core electrons act on the valence electrons and to take into account the relativistic effects of the heavy Pb core. Relaxation of flat terraces and of step atoms were calculated using a conjugate gradient method in the optimizer LoptCG which is designed to work with the Crystal98 code.

For the calculation of the STM images and the structure optimizations, a hybrid method of the density functional theory (DFT) and Hartree-Fock (HF) approach was applied (Becke3LYP option in Gaussian98). The exchange is described by a mixture of HF-exchange and a Lee, Yang and Parr (LYP)-type density functional, whereas the correlation is provided by a combination of LYP-terms (local correlation) and Vosko, Wilk, and Nusair (VWN, excess local correlation) terms. This hybrid method usually gives the most precise results for cluster geometries of semiconducting and insulating materials (Fox, personal communication; Gibbs et al. 1999). In addition, this method is computationally faster and sturdier than pure DFT calculations.

RESULTS

Experimental STM images

Figure 1 shows in vacuum STM images of a clean galena (100) surface including a half unit cell high step with several kinks taken at positive bias voltage (0.25 V, set point current = 1 nA). The topographic image (Fig. 1a) shows atomic corrugation across a (100) terrace up to the step edge. At the step edge, an increase in the apparent height is displayed relative to the average level of the terrace sites, and individual atomic sites at the step edge are less clearly distinguished than sites across the terrace. In the absence of other information, the apparent height increase at the step edge could be interpreted as a change in the atomic structure, or as a change in the electronic structure, or a combination of the two. Atomic corrugation is also seen in the current image (Fig. 1b), which is more easily resolved because the full grayscale contrast range has been applied to the entire atomic corrugation, whereas in Figure 1a, it is applied to the step edge which dominates the surface topography. The current image gives an indication that the tunneling current is higher at step edge sites, but as will be discussed below, this indication is less meaningful than the indication given in the topographic image. As shown by Becker and Hochella (1996), and by using a somewhat more optimized basis set in Figure 2a, the conduction band density that is picked up by STM images using a positive sample bias is dominated by Pb $6p_z$ states such that the bright spots on flat terraces are located above Pb atoms. However, as indicated in Figure 1c, the apparent Pb-Pb angle where the first and third Pb are in an atomic row closer to the step open up from 90° to approximately 120° in the row next to the step. Collectively, the image data suggest that two characteristics are associated with the step edges on galena (100). The first is a change in the atomic or electronic

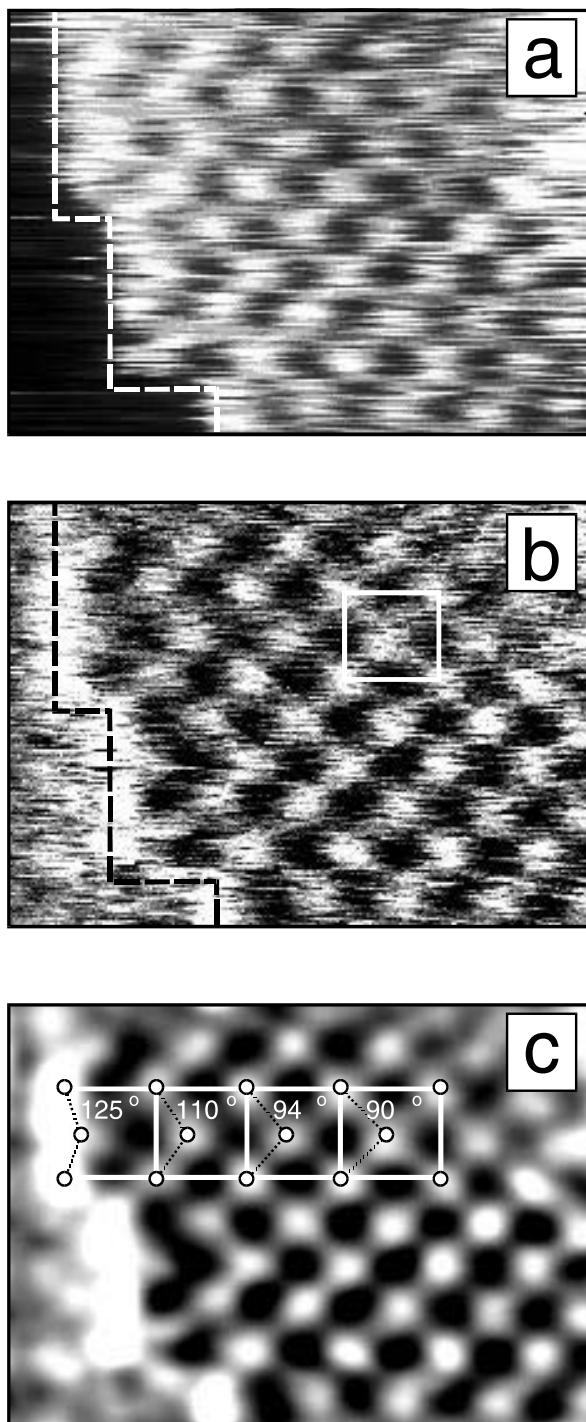


FIGURE 1. (a) Topographic image of a galena surface taken at 0.25 V sample bias voltage and 1 nA setpoint current. The image shows a galena surface with a step and several kink sites. An increased tunneling current is localized along the step edge sites, causing them to be less distinguishable than terrace atoms. The bright spots on flat terraces correspond mainly to $Pb6p_z$ -like states that are located above surface Pb atoms. (b) Unfiltered current image for the area of the surface shown in a. (c) FFT filtered current image that shows the apparent changes in the structure of the terrace in the proximity of the step edge. The apparent widening of the Pb-Pb-Pb angle is labeled which is mainly a result of the modified electronic structure of the surface near steps rather than atomic relaxation.

served tunneling current distribution near the step edge is present in the images because the tip did not properly negotiate the topographic height increase encountered at the step edge. In the ideal limit for situations where a step edge is to be imaged, where the tip response to such features is perfect (i.e., a constant tunneling current is always maintained), any true increased tunneling current at step edge sites would be displayed in the topographic image as an increase in the apparent height (Fig. 1a) while the current image (the error signal) would be featureless (Figs. 1b and 1c). For a condition where the tip response is not perfect, artifacts may appear in the images. One such artifact is a false increased tunneling current at the step edge in the current image, arising because at that location the tip briefly passed closer to step edge atoms before correcting its course. In a case where no increased tunneling current is actually associated with step edge sites, this would not be a reflection of the true electronic structure. In topographic images, this unwanted deviation in the tip path can make the step edge appear smoother than it is. In our images, the ideal limit was not attained, which is routinely the case in STM studies at the atomic scale. If the ideal limit was attained, then the images in Figures 1b and 1c would be featureless. This means that the increased tunneling current at the step edge displayed in Figures 1b and 1c are artifacts to some degree. However, we can argue that the images were collected close enough to the ideal limit. There is no obvious step edge smoothing in the topographic image, so we can make the assumption that the atomic structure at the step edge is close to ideal (a pure step function). This assumption is supported by previous work (e.g., Wright et al. 1999a, 1999b) and results presented below. Also, the presence of this type of artifact suggests that the apparent height increase observed at the step edge in the topographic image (Fig. 1a) may actually be somewhat underestimated. Therefore, because the apparent height increase at the step edge is recorded in the topographic image, it can be concluded that this is a real characteristic of the step edge. The artifacts are thus inconsequential to the conclusions of this study.

Theoretical STM images

To understand these observations of the electronic structure, we used a cluster calculation designed to model the [100] step edge environment. We set up a cluster with six atomic rows parallel and perpendicular to the step, and two atomic layers at the lower terrace and three at the upper terrace as shown in Figure 2b. As described in the Methods section, this setup also contains embedding point charges on the sides and

structure at step edge sites. The second is an apparent deformation in the arrangement of atoms in nanometer proximity to step edges.

It is important to consider the possible contribution of scanning artifacts to the image data. In this case, it is crucial because each row of the image was collected with the tip scanning from left to right, which introduces the possibility that the ob-

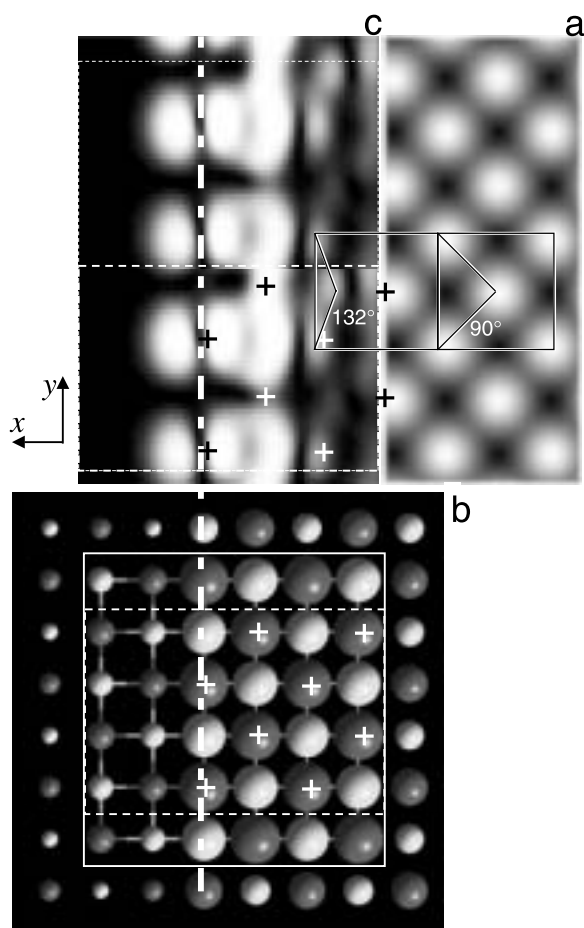


FIGURE 2. (a) Calculated constant height STM image for a flat terrace with periodic boundary conditions using Crystal98. (b) Setup for a cluster calculation of a theoretical STM image as shown in c. The cluster consists of 6×6 atoms with 3 atomic layers on the upper terrace (larger balls; bright balls = S and dark balls = Pb) and 2 atomic layers on the lower terrace (smaller balls). Indicated are also the embedding point charges that are located at lattice positions around and below the cluster (outside the solid square). The values of the embedding point charges are calculated using the method described in Becker et al. (1997a). (c) Calculated STM image for a bias voltage of +0.25 V using the cluster setup in b. In brief, in constant current mode, the tip positions are calculated and averaged over y and over 1 \AA in the $\pm x$ direction. The tip is scanned along this surface and the tunneling current calculated as a function of (x,y) . No surface relaxation is applied. The image is calculated for the area represented by the dashed rectangle (in b and c) and repeated for better graphical representation. The fine grid in the image represent the lateral positions of the tip for which the STM image was calculated. Surface Pb atoms on the upper terrace are indicated by “+” signs. Parts a and c are aligned such that the lattice is continuous.

below the cluster to minimize edge effects. To further reduce edge effects, the area for which the STM image was calculated is smaller than the actual cluster (see dashed rectangles in Figs. 2b and 2c) and is then repeated in Figure 2b for a better graphical representation of the electronic structure near the step. At this time we are not able to run calculations on a cluster or a periodic unit cell large enough to mimic the whole surface area that is shown in the experimental image in Figure 1 because

the computational expense of these types of calculations increases with the number of atoms to the power of approximately 3. However, the combination of a periodic calculation (Fig. 2a, for the extreme case of being infinitely far away from a step) and a cluster calculation (Fig. 2b and 2c) representing the electronic structure close to the step allows us to capture most of the features shown in the experimental image. First, one can see how the apparent Pb-Pb-Pb angle (denoted as an 132° angle in Fig. 2c) opens up in the third to last row before the step on the upper terrace. It should be noted that all atoms in the cluster were kept frozen at unrelaxed lattice positions in order to determine whether this is solely an electronic effect or a combination of electronic and atomic relaxation in the near step region. The reduction in the lateral symmetry due to the step has a far reaching influence on the shape of the orbitals several atomic rows away from the actual step site. As will be discussed later in the Atomic Relaxation section, this is for the most part an electronic effect rather than the result of atomic relaxation. Further, our calculations show that the area of high empty state density close to the Fermi level begins in the second to last row before the step on the upper terrace. Now, if the (theoretical) tip moves closer to and beyond the step, a new pattern of the electronic structure emerges. About 2 \AA beyond the step on the side of the lower terrace, another maximum of the tunneling current from the tip to the sample appears. This maximum is a superposition of a Pb $6p_x$ -like state (x defined as being perpendicular to the step) of a Pb atom at the top of the step and a Pb $6p_z$ -like state of the Pb atom located in the next atomic row at the bottom of the step. This feature is also visible in the experimental images as a “frayed” state density on the side of the lower terrace whereas the maximum of the state density on the side of the upper terrace is almost terminated by a straight line (Fig. 1b and 1c).

The described effects of surface symmetry reduction near a step were found to be highly suppressed when the step is modeled as a two-dimensional periodic array with single PbS rows removed on the surface. In order to create a periodic supercell for the simulation with Crystal98, we removed every fourth surface row (Figs. 3a and 3b) and calculated the density of states at the top of the valence band and at the bottom of the conduction band. This information was used to calculate constant height STM images (Fig. 3c). In this model, there is a perturbation of the electronic structure of the “ridges” formed by the uppermost atomic plane (three atomic rows wide) arising from two steps on both sides of a ridge. Interestingly, the symmetry reducing effects from these two steps on the electronic structure cancel each other such that we only find maxima of the state density directly above the atoms as on flat terraces. Because we learned from Figure 2c that the increase in the density of states begins about one atomic row away from the step, the “ridges” in Figure 3 are not wide enough to show the complete dropoff in state density from a step to a terrace.

Electron density of states of the bulk, flat, and stepped terraces

Figure 4 shows the total and projected density of states of the top of the valence band and the lower 7 eV of the conduction band of bulk galena. In this representation, the band gap,

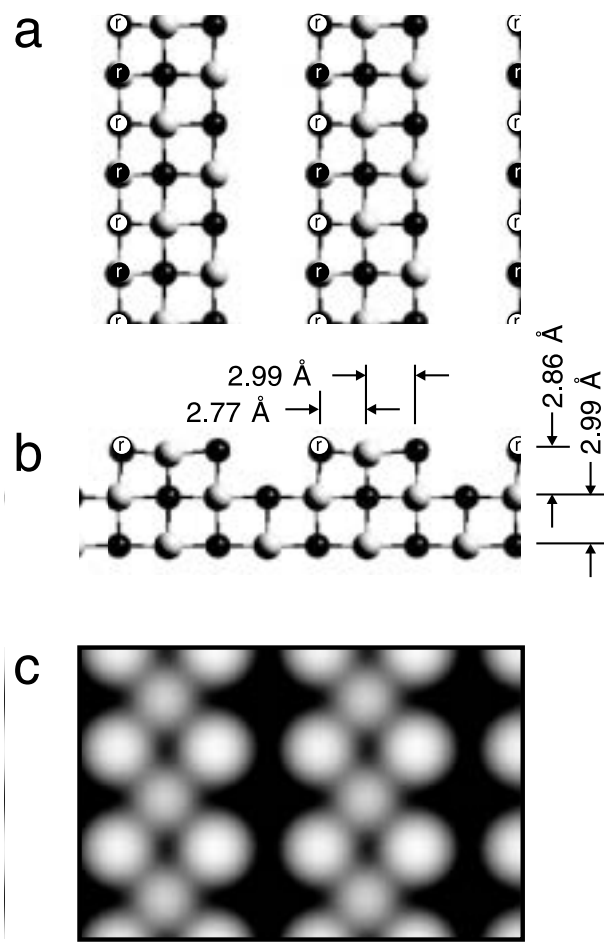


FIGURE 3. (a) Top view (only the uppermost layer is shown) and (b) side view of an atomic relaxation calculation where only the atoms labeled “r” were allowed to relax. The amounts of vertical and lateral relaxations are described in the text. (c) Calculated constant height STM image for a bias voltage of +0.5 V for the setup shown in **a** and **b**.

visible as a flat line left and right of the Fermi level, is overestimated (~ 1.2 eV) when compared with experimental values which are on the order of 0.3 to 0.5 eV (Tossell and Vaughan 1987, and references therein). This is due to the nature of the one-electron/mean-field computational approach, inherent to both DFT and HF methods, which is not capable of leading to an accurate estimation of band gap widths (Tossell and Vaughan 1992). Both the top of the valence band and the bottom of the conduction band consist of states with S 3p and Pb 6p character with S 3p dominating the top of the valence band and Pb 6p the bottom of the conduction band. Therefore, spots of high state density in STM images are located above S atoms for negative bias voltages and above Pb atoms for positive bias voltages. The Pb 6s peak lies deep in the valence band because of the relativistic stabilization of the 6s electron pair. This effect also has chemical importance such that this “inert pair”

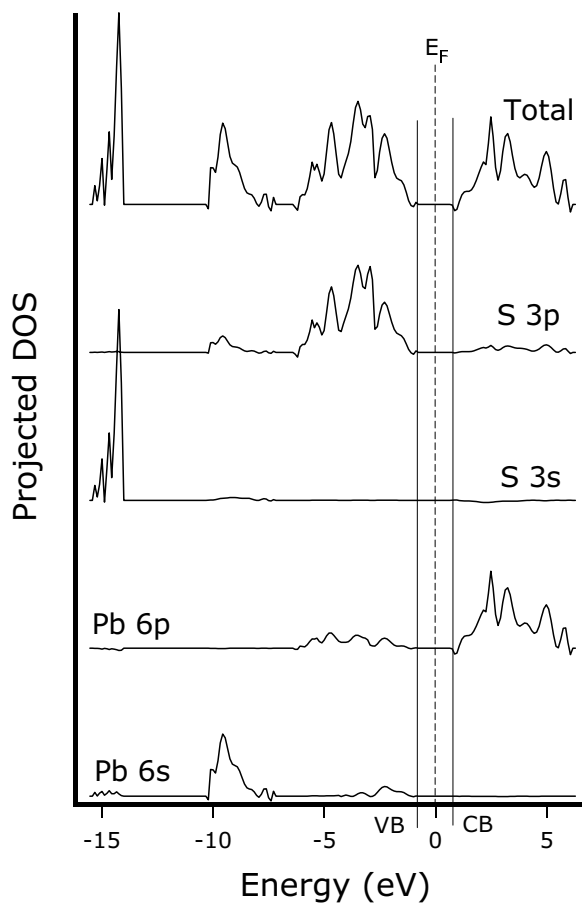


FIGURE 4. Total and projected density of states of bulk galena using three-dimensional periodic boundary conditions calculated with Crystal98. The band gap is indicated by straight vertical lines with the Fermi level E_F within the band gap and the valence band (VB) on the left and the conduction band (CB) on the right of the band gap.

effect for heavy elements is believed to be the reason for why elements such as Hg, Tl, Pb, and Bi can seldom occur in oxidation states higher than +2 (Jolly 1991).

When we compare the density of states projected to surface S 3p and Pb 6p states (Fig. 5a) with the respective bulk-like states, we find that the DOS increases for surface states when their energy eigenvalues are close to the Fermi level. This effect is more pronounced when we make the transition from surface-like to step-like states (Fig. 5b). This is important because the states that are close to the Fermi level are the ones that are involved in redox reactions. The increase of the DOS at sites that are less coordinated than sites on flat terraces is another explanation why steps are usually more reactive than terraces, especially for adsorption reactions involving electron transfer. In contrast, the bulk DOS is more concentrated at states deeper in the valence band or higher in the conduction band than the terrace or step DOS. It is interesting to note that the energy eigenvalues for the bulk, terrace, and step sites are at the same positions (this is exactly true if bulk, surface, and

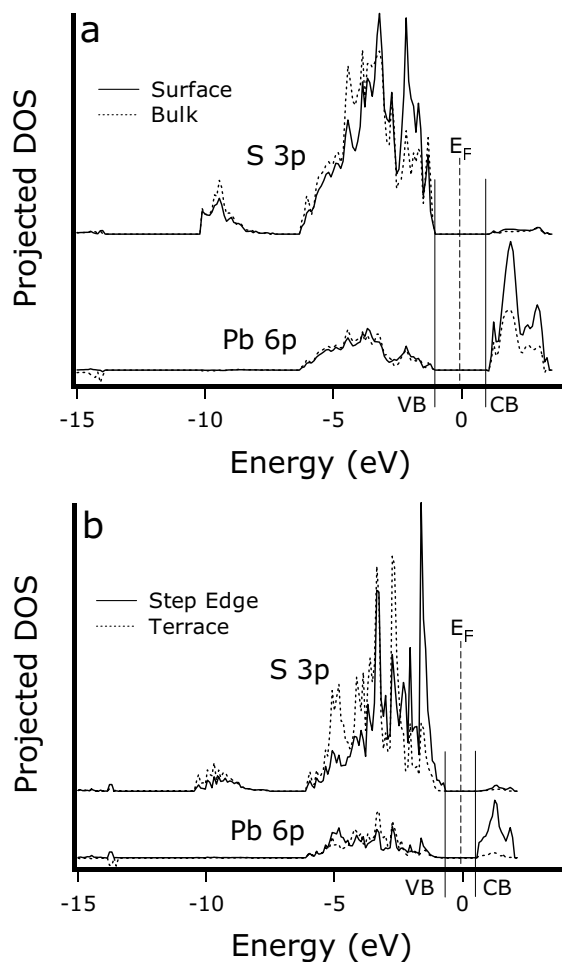


FIGURE 5. Projected density of states (*S 3p* and *Pb 6p* like states) of (a) a periodic slab (with a comparison of projections to bulk-like and terrace-like states) and (b) a periodic slab with a “groove”-like (see Fig. 5) periodic step (with a comparison of projections to terrace-like and step-like states). E_F , *VB*, and *CB* here the same meaning as in Figure 4.

step states are modeled in the same computational setup). This is not surprising because each state in a crystal is represented by a Bloch function. These Bloch functions have the periodicity of the lattice (if there are perturbations to the lattice such as defect sites, the number of Bloch functions has to be increased but the general scheme still holds true). Thus, each of these functions “travels” through the whole crystal with different densities at different positions but each is represented by a single energy value. This explains why we obtain peaks for different projections at the same position but with different heights in Figures 4 and 5.

It is interesting to note that the apparent band gap decreases from Figure 5a to Figure 5b. Even though the Becke3LYP method underestimates the band gap of semiconductors, comparison of both figures suggests that the introduction of steps creates “step states” (analogous to the often described surface states that can be located in the bulk band gap).

Atomic relaxation

As previously described by Becker and Hochella (1996), and by recent experimental work (e.g., Leiro et al. 1998), there is little relaxation on flat *PbS* (100) terraces. Our calculations in this study with a more optimized basis set and taking electron correlation effects into account confirm this finding. There is a small vertical rumpling which means that the distance of a surface *Pb* to an underlying *S* is reduced from 2.99 Å (experimental value 2.96 Å) to 2.95 Å and the corresponding surface *S* to *Pb* distance from 2.99 Å to 2.86 Å. The lateral relaxation is calculated to be zero.

The situation is different at steps. The vertical distance of a surface step *Pb* to the *S* atom underneath is reduced to 2.9 Å and the separation of a surface step *S* to the underlying *Pb* to 2.7 Å (Figs. 3a and 3b). As derived from cluster calculations, atoms at corner sites will be drawn another 0.2 Å towards the underlying substrate. In addition, with the setup in Figures 3a and 3b, we calculated a lateral contraction of step atoms of about 0.22 Å towards the upper surface. The vertical contraction of the uppermost atomic plane, and the lateral contraction of the step edge atoms demonstrate similarities in both the relaxation behavior of the undercoordinated atoms (a contraction) and displacement magnitude. This behavior is consistent with observed trends for the cubic surfaces of many ionic and covalent minerals based on the rocksalt structure, which also indicate that almost all of the relaxation displacement is restricted to the outermost atoms (Noguera 1996; Gibson and LaFemina 1996). Therefore, the optimized surface structures for the models used in this study are likely to have released the vast majority of the strain present in the initial unrelaxed surface.

It is interesting to note that this lateral relaxation is far less than what one would expect from the experimental image in Figure 1, if the bright spots in the image are interpreted as positioned directly above atomic sites. Thus, by taking into account the calculated image in Figure 2c and the atomic relaxation in Figure 3, it becomes obvious that the apparent change in the *Pb-Pb-Pb* angle as observed by STM (Fig. 1c) is predominantly an electronic effect and little can be attributed to atomic relaxation.

DISCUSSION

The results of this study allow us to put forward an explanation for the known reactive behavior of *PbS* surfaces and the catalytic properties of step edge sites, specifically in regard to acid/base interactions with H_2O . A complete understanding of the acid/base behavior of surface sites is based on a complicated set of interrelated factors such as the ability to receive or donate electrons (charge transfer) and adsorption energies (Noguera 1996). Here, we consider specifically charge transfer, because it is the principal factor that drives the weakening of the O-H bond in a sorbed H_2O molecule. The latter is largely the control on protonation or Brønsted-type reactions at surfaces. The charge transfer behavior of a surface site can be viewed in terms of Lewis acidity/basicity, where a site that readily accepts electrons is a Lewis acid. In this context, the site acidity is increased by increasing its ability to accept and lower the energy of the donated electrons. As an H_2O molecule

approaches a surface site, its orbitals overlap with the accessible orbitals at the surface and the valence electrons are affected by the potential of one other. The Fermi levels of the two equalize, with charge transfer directed from the highest occupied states to the lowest unoccupied states. Weakening of an O-H bond, the precursor step to hydrolysis, is achieved by either decreasing the occupation of bonding sp^3 -like orbitals or by increasing the occupation of antibonding orbitals in H_2O . Wright et al. (1999a, 1999b) have shown that the negative end of the H_2O dipole interacts strongly with step edge Pb sites, causing a lengthening of the O-H bond. Our results clearly show that the density and energy of empty Pb 6p states is significantly increased at step edge Pb sites relative to that of terrace Pb sites. The former can be viewed as increasing the capacity to accept electrons and the latter can be viewed as increasing the driving force to accept them. Collectively, a consistent picture emerges involving charge transfer from the sorbed H_2O molecule to step edge Pb sites, via σ -like interaction between sp^3 and 6p orbitals in the surface adduct group.

Geometric considerations can also exert a potentially important influence on the propensity for sorbed H_2O to dissociate. The fact that the main maximum of empty state density is on the upper terrace, approximately one row away from the actual step edge plane, could mean that H_2O would preferentially adsorb at the upper terrace of the step rather than the lower terrace. This would be in contrast to many mineral surfaces where the lower terrace is an energetically preferred adsorption site because the adsorbed species can coordinate to atoms at the lower and upper terrace. H_2O adsorption to a step could lead to a higher probability for hydrogen bonds to form with surrounding surface sites, affecting the O-H bond strength and the tendency to dissociate. The calculations by Wright and co-workers seem to suggest that hydrogen bonding is not important in the precursor complex, but are formed in the transition state of dissociation.

In addition, we have to consider the effect of the step electronic structure on nucleophilic adsorption of metal atoms to step or near step sites. In analogy to the water adsorption, nucleophilic species could adsorb at the upper terrace of the step rather than the lower terrace. Such a nucleophilic species could, for example, be a neutral metal atom that is less electronegative than the sulfide surface (e.g., Ag, Au). If we imagine such a metal atom to undergo surface diffusion on the upper terrace, it may eventually bond at the described maximum of conduction band state density near the step. At higher surface metal concentrations, this effect can lead to the formation of metal clusters or ridges along the surface. How far reaching the influence of a surface defect such as a step, kink, or vacancy can be is described by Rosso et al. (2000). In contrast, a species diffusing on the lower terrace may eventually bond to the other maximum of conduction band density which is located on the side of the lower terrace of the step (Figs. 1 and 2).

Finally, we consider the importance of the conclusion that, at PbS step edges, the electronic structure deforms more significantly than the atomic positions. This observation is not unlike that documented by Eggleston and Hochella (1992) in an ambient STM investigation of step edges on pyrite (FeS_2) (100) in oil. The findings are suggestive of the long-range in-

fluence structural defects may have on the shapes and energies of the frontier orbitals at the surface and therefore the surface reactivity. In this way, defects can exert a "remote" influence on sorbates interacting with sites nearby (Rosso et al. 2000; Becker et al. 2001). That the structure local to one site can link with the structure of another on the scale of a few tens of Ångströms should be considered paramount to understanding individual site behavior on these and other semiconducting mineral surfaces.

ACKNOWLEDGMENTS

U.B. is grateful for financial support from the Deutsche Forschungsgemeinschaft (DMG, Habilitationstipendium 1952/1-1.3). Pacific Northwest National Laboratory is operated for the Department of Energy by Battelle Memorial Institute under Contract DE-AC06-76RLO 1830. We appreciate the careful and inspiring reviews and suggestions by Steve Higgins and an anonymous reviewer.

REFERENCES CITED

- Becker, U. and Hochella, M.F. Jr. (1996) The calculation of STM images, STS spectra, and XPS peak shifts for galena: New tools for understanding mineral surface chemistry. *Geochimica et Cosmochimica Acta*, 60, 2413–2426.
- Becker, U., Hochella, M.F. Jr., and Aprà, E. (1996) The electronic structure of hematite {001} surfaces: Applications to the interpretation of STM images and heterogeneous surface reactions. *American Mineralogist*, 81, 1301–1313.
- Becker, U., Greatbanks, S.P., Rosso, K.M., Hillier, I.H., and Vaughan, D.J. (1997a) An embedding approach for the calculation of STM images: Method development and application to galena (PbS). *Journal of Chemical Physics*, 107, 7537–7542.
- Becker, U., Vaughan, D.J., and Hochella, M.F. Jr. (1997b) The adsorption of gold to galena surfaces: Calculation of adsorption/reduction energies, reaction mechanisms, XPS spectra, and STM images. *Geochimica et Cosmochimica Acta*, 61, 3565–3585.
- Becker, U., Rosso, K.M., and Hochella, M.F. Jr. (2001) The proximity effect on semiconducting mineral surfaces: A new aspect of mineral surface reactivity and surface complexation theory? *Geochimica et Cosmochimica Acta*, (in press).
- Bosbach, D. and Hochella, M.F. (1996) Gypsum growth in the presence of growth inhibitors: A scanning force microscopy study. *Chemical Geology*, 132, 227–236.
- Bosbach, D., Jordan, G., and Rammensee, W. (1995) Crystal growth and dissolution kinetics of gypsum and fluorite—an in-situ scanning force microscope study. *European Journal of Mineralogy*, 7, 267–276.
- Bosbach, D., Junta-Rosso, J.L., Becker, U., and Hochella, M.F. Jr. (1996) Gypsum growth in the presence of background electrolytes studied by Scanning Force Microscopy. *Geochimica et Cosmochimica Acta*, 60, 3295–3304.
- Botner, R., Ratz, S., Schroeder, N., Marquardt, S., Gerhardt, U., Gaska, R., and Vaitkus, J. (1996) Analysis of angle-resolved photoemission data of PbS (001) surfaces within the direct-transition model. *Physical Review B—Condensed Matter*, 53, 10336–10343.
- Bryce, R.A., Vincent, M.A., Hillier, I.H., and Hall, R.J. (2000) Structure and stability of galena (PbS) at the interface with aqueous solution: a combined embedded cluster/reaction field study. *Journal of Molecular Structure—Theochem*, 500, 169–180.
- Dove, P.M. and Hochella, M.F. (1993) Calcite precipitation mechanisms and inhibition by orthophosphate—in-situ observations by scanning force microscopy. *Geochimica et Cosmochimica Acta*, 57, 705–714.
- Dove, P.M. and Platt, F.M. (1996) Compatible real-time rates of mineral dissolution by Atomic Force Microscopy (AFM). *Chemical Geology*, 127, 331–338.
- Dovesi, R., Saunders, V.R., Roetti, C., Causà, M., Harrison, N.M., Orlando, R., and Aprà, E. (1999) Crystal98, an ab initio Hartree-Fock LCAO program for periodic systems. University of Turin, Italy.
- Eggleston, C.M. (1997) Initial oxidation of sulfide sites on a galena surface: Experimental confirmation of an ab-initio calculation. *Geochimica et Cosmochimica Acta*, 61, 657–660.
- Eggleston, C.M. and Hochella, M.F. (1992) Scanning tunneling microscopy of pyrite (100) — surface structure and step reconstruction. *American Mineralogist*, 77, 221–224.
- (1993) Tunneling spectroscopy applied to PbS (001) surfaces: fresh surfaces, oxidation, and sorption of aqueous Au. *American Mineralogist*, 78, 877–883.
- (1994) Atomic and electronic structure of PbS (100) surfaces and chemisorption oxidation reactions. ACS Symposium Series, 550, 201–222.
- Eggleston, C.M., Ehrhardt, J.J., and Stumm, W. (1996) Surface structural controls on pyrite oxidation kinetics: An XPS-UPS, STM, and modeling study. *American Mineralogist*, 81, 1036–1056.

- Fowler, T.A. and Crundwell, F.K. (1999) Leaching of zinc sulfide by *Thiobacillus ferrooxidans*: Bacterial oxidation of the sulfur product layer increases the rate of zinc sulfide dissolution at high concentrations of ferrous ions. *Applied and Environmental Microbiology*, 65, 5285–5292.
- Frisch, M.J. et al. (1998) Gaussian 98, Revision A.7. Gaussian, Inc., Pittsburgh, Pennsylvania.
- Gibbs, G.V., Tamada, O., Boisen, M.B., and Hill, F.C. (1999) Laplacian and bond critical point properties of the electron density distributions of sulfide bonds: A comparison with oxide bonds. *American Mineralogist*, 84, 435–446.
- Gibson, A.S. and LaFemina, J.P. (1996) Structure of mineral surfaces. In P.V. Brady, Ed. *Physics and Chemistry of Mineral Surfaces*, p. 1–62. CRC Press, Boca Raton, Florida.
- Higgins, S.R. and Hamers, R.J. (1995) Spatially resolved electrochemistry of the lead sulfide (galena) (001) surface by electrochemical scanning tunneling microscopy. *Surface Science*, 324, 263–281.
- (1996a) Morphology and dissolution processes of metal sulfide minerals observed with the electrochemical scanning tunneling microscope. *Journal of Vacuum Science and Technology*, B 14, 1360–1364.
- (1996b) Chemical dissolution of the galena(001) surface observed using electrochemical scanning tunneling microscopy. *Geochimica et Cosmochimica Acta*, 60, 3067–3073.
- Holmes, P.R., Fowler, T.A., and Crundwell, F.K. (1999) The mechanism of bacterial action in the leaching of pyrite by *Thiobacillus ferrooxidans*. *Journal of the Electrochemical Society*, 146, 2906–2912.
- Jolly, W.L. (1991) *Modern Inorganic Chemistry*, Second Edition, McGraw-Hill, Inc., New York.
- Jordan, G. and Rammensee, W. (1996) Growth and dissolution on the CaF₂ (111) surface observed by scanning force microscopy. *Surface Science*, 371, 371–380.
- (1998) Dissolution rates of calcite (1014bar) obtained by scanning force microscopy: Microtopography-based dissolution kinetics on surfaces with anisotropic step velocities. *Geochimica et Cosmochimica Acta*, 62, 941–947.
- Junta, J. and Hochella, M.F. (1994) Manganese (II) oxidation at mineral surfaces – A microscopic and spectroscopic study. *Geochimica et Cosmochimica Acta*, 58, 4985–4999.
- Laajalehto, K., Smart, R.S., Ralston, J., and Suoninen, E. (1993) STM and XPS investigation of reaction of galena in air. *Applied Surface Science*, 64, 29–39.
- Leiro, J.A., Laajalehto, K., Kartio, I., and Heinonen, M.H. (1998) Surface core-level shift and phonon broadening in PbS(100). *Surface Science*, 413, L918–L923.
- Maier, G.S. and Dobias, B. (1997) 2-mercaptobenzothiazole and derivatives in the flotation of galena, chalcocite and sphalerite: A study of flotation, adsorption and microcalorimetry. *Minerals Engineering*, 10, 1375–1393.
- Mian, M., Harrison, N.M., Saunders, V.R., and Flavell, W.R. (1996) An ab initio Hartree-Fock investigation of galena (PbS). *Chemical Physics Letters*, 257, 627–632.
- Noguera, C. (1996) *Physics and Chemistry at Oxide Surfaces*. 223 p. Cambridge University Press, Cambridge.
- Persson, I. (1994) Adsorption of ions and molecules to solid surfaces in connection with flotation of sulfide minerals. *Journal of Coordination Chemistry*, 32, 261–342.
- Pina, C., Becker, U., Risthaus, P., Bosbach, D., and Putnis, A. (1998) Molecular scale mechanisms of crystal growth in barite. *Nature*, 395, 483–486.
- Risthaus, P., Bosbach, D., Becker, U., and Putnis, A. (2001) Barite scale formation and dissolution at high ionic strength studied with Atomic Force Microscopy. *Colloids and Surfaces A: Physicochemical and Engineering Aspects*, in press.
- Rosso, K.M., Becker, U., and Hochella M.F. Jr. (1999a) Atomically resolved electronic structure of pyrite {100} surfaces: an experimental and theoretical investigation with implications for reactivity. *American Mineralogist*, 84, 1535–1548.
- (1999b) The oxidation of pyrite {100} surfaces with O₂ and H₂O: fundamental oxidation mechanisms. *American Mineralogist*, 84, 1549–1561.
- (2000) Surface defects and self-diffusion on pyrite {100} using ultra-high vacuum scanning tunneling microscopy and theoretical modeling. *American Mineralogist*, 85, 1428–1436.
- Santhiya, D., Subramanian, S., and Natarajan, K.A. (2000) Surface chemical studies on galena and sphalerite in the presence of *Thiobacillus thiooxidans* with reference to mineral beneficiation. *Minerals Engineering*, 13, 747–763.
- Sampson, M.I., Phillips, C.V., and Ball, A.S. (2000) Investigation of the attachment of *Thiobacillus ferrooxidans* to mineral sulfides using scanning electron microscopy analysis. *Minerals Engineering*, 13, 643–656.
- Sharma, P.K. and Rao, K.H. (1999) Role of a heterotrophic *Paenibacillus polymyxa* bacteria in the bioflotation of some sulfide minerals. *Minerals & Metallurgical Processing*, 16, 35–41.
- Stipp, S.L.S., Eggleston, C.M., and Nielsen, B.S. (1994) Calcite surface structure observed at microtopographic and molecular scales with atomic force microscopy (AFM). *Geochimica et Cosmochimica Acta*, 58, 3023–3033.
- Teng, H.H. and Dove, P.M. (1997) Surface site-specific interactions of aspartate with calcite during dissolution: Implications for biomineralization. *American Mineralogist*, 82, 878–887.
- Tossell, J.A. and Vaughan, D.J. (1987) Electronic structure and the chemical reactivity of the surface of galena. *Canadian Mineralogist*, 25, 381–392.
- (1992) *Theoretical geochemistry: applications of quantum mechanics in the earth and mineral sciences*. Oxford University Press, New York.
- Vaitkus, J., Kazlauskienė, V., Miskinis, J., and Sinius, J. (1998) PbS thin film formation on terrace-step surface by pulsed laser deposition. *Materials Research Bulletin*, 33, 711–716.
- Vaitkus, J., Baubinas, R., Gaubas, E., Kazlauskienė, V., Miskinis, J., Mazeikis, A., Sinius, J., Zasiņas, E., and Zindulis, A. (1999) Cluster and thin layer of compound semiconductor growth on hexagonal and vicinal cubic surface and the simulation of atom behavior. *Microelectronics Journal*, 30, 335–340.
- Wang, J., Hu, Y.H., Qiu, G.Z., and Zhong, K.N. (2000) Mechanism of silver-influenced bacterial leaching of chalcopyrite, pyrite and a copper ore. *Transactions of the Nonferrous Metal Society of China*, 10, 71–75.
- Wieland, A. and Kuhl, M. (2000) Short-term temperature effects on oxygen and sulfide cycling in a hypersaline cyanobacterial mat (Solar Lake, Egypt). *Marine Ecology, Progress Series*, 196, 87–102.
- Woods, R. (2000) Recent advances in electrochemistry of sulfide mineral flotation. *Transactions of Nonferrous Metals Society of China*, 10, 26–29.
- Wright, K., Hillier, I.H., Vaughan, D.J., and Vincent, M.A. (1999a) Cluster models of the dissociation of water on the surface of galena (PbS). *Chemical Physics Letters*, 299, 527–531.
- Wright, K., Hillier, I.H., Vincent, M.A., and Kresse, G. (1999b) Dissociation of water on the surface of galena (PbS): A comparison of periodic and cluster models. *Journal of Chemical Physics*, 111, 6942–6946.

MANUSCRIPT RECEIVED SEPTEMBER 18, 2000

MANUSCRIPT ACCEPTED FEBRUARY 25, 2001

MANUSCRIPT HANDLED BY S.L.S. STIPP